Study of Bacterial L-asparaginase and Molecular expression of l-asparaginase gene in Escherichia coli

Dr. Luay Mannaa Ibrahim

Northern technical university / Al-dour technical institute /
dr.luay.m.ibrahim@ntu.edu.iq

Abstract

E. coli remains highly active even after it is removed from the blood, possibly by sequestration by liver cells) the half-life of the enzyme is increased when lymphoma cells are implanted in guinea pigs. Since then, several microorganisms were evaluated to obtain an L-asparaginase with greater antitumor activity compared to that produced by *E. coli* and that was produced in an economically viable way. It is considered that the new L-asparaginases to be used as medication must have pharmacological activity causing minimal side effects. Thus, it is expected that they present a high affinity for the substrate, a half-life time sufficient to avoid administration of several doses, low immunogenicity and high stability. It was also postulated that a low cross-glutaminolytic activity is important to avoid excessive side effects of the enzyme treatment. Various information can be extracted from the simulation trajectory, such as the energy of interaction between residues from the catalytic site of an enzyme and its substrate (intermolecular) or interactions that one or more generated mutations may have with neighboring residues within the protein (intramolecular) .In the Total Potential Energy equation, we can see that the first three terms refer to: the bond length, the angles between the atoms and the bond twist, respectively. The fourth term of the equation refers to the calculation for non-directly bonded atoms and for atoms whose interaction is intermolecular, thus considering the van der Waals and Coulomb interactions.

Introduction

The *E. coli* enzyme has already had its crystallographic quaternary structure resolved. There are 8 crystallographic structures deposited in the Protein Data Bank - PDB, and

among these, the most used in analysis is the one that receives the 3ECA code. Residues 1-190 are located in the N-terminal domain, linked through residues 191-212 to the C-terminal domain, formed by residues 213-326 (Lopes et al, 2017).

The specific activity of the enzyme for Asn is 280-400 international units per milligram of pure protein (I.U./mg), with KM of 12 µM and isoelectric point 5.0; the KM for glutamine is 3000 µM.

There are several techniques for quantifying the L-asparaginase enzyme. Methods employing chromatographic analysis of amino acids, colorimetric reactions with ninhydrin and fluorometric reactions quantifying the formation of 7-amino-4-methylcoumarin were developed (Verma et al., 2007). However, the standard method for direct quantification of the L-asparaginase enzyme is still the Nessler method. This method is based on the quantification of the ammonium released during the asparaginolysis reaction through the Nessler reagent, an alkaline solution of 2.5 mol.L-1 potassium tetraiodomercurate. The reaction of ammonium with potassium tetraiodomercurate generates an orange color, which can be read in a spectrophotometer at 436 nm (Wriston; Yellin, 1973).

Another effective methodology for quantifying L-asparaginase activity is the hydroxylamine technique. It is based on the ability of L-asparaginase to convert the amino acid L-asparagine to β-hydroxyl aspartic acid (AHA) when in contact with hydroxylamine hydrochloride. Then AHA reacts with $FeCl_3$, forming a reddish color that can be quantified in a spectrophotometer at 500 nm. Several authors used this methodology to quantify the asparaginolytic activity in situations where the interferers end up making the Nessler method unfeasible (Oliveira et al., 2003).

L-asparaginase studied in this study is the main enzyme commonly used in cancer chemotherapy. The mechanism of action of the enzyme, which is found only in some gram-negative bacteria with this activity, is based on the deprivation of this exogenous amino acid by cancer cells, which are auxotrophic in terms of L-asparagine. Normal cells that are prototrophs for this amino acid are not affected by such an application, since they have an active enzyme L-asparagine synthetase. The physical and chemical conditions

required for the optimization of the production of L-asparaginase, which is of great industrial importance, by different bacteria belonging to the same group were investigated. For this, vgb was cloned and Pseudomonas aeruginosa and Enterobacter aerogenes, which are known for their ability to produce this enzyme, as well as the ansB gene were cloned and *E. coli* HB101 [pAHZ12] and Enterobacter aerogenes [pB-PGA] bacteria that we cloned were used. In particular, very different results have been reported on the oxygen and carbon catabolite repression of the enzyme. For example, while some studies on closely related bacterial species have reported that oxygen suppresses the production of this enzyme, in others there are findings that oxygen increases enzyme production. There is no doubt that recombinant bacteria equipped with an efficient oxygen uptake system will clarify such a controversial issue.

Materials and Methods

PCR was amplified using forward and reverse primers with nucleotide sequences (fw) 5 '-ATCGGATCCATCACCATT-3' and (rv) 5 'GCGAAGTTTAGTTAGATGATGATT-3' respectively with a complete open reading frame (ORF) of the L-asparaginase (L-ASP) gene from *Psychrobacter cryohalolentis* (Pcryo_0631) comprising gene consisting of 919 bp. At the ends of ORF the sites were introduced for restrictive enzymes *Bam*HI and *Hind*III. Initially, the PCR product was cloned with the CloneJET PCR cloning kit by pET-28a plasmid vector (Catalogue No. K1232 - Thermo Scientific TM). In the LB broth, bacterial colonies were successfully transformed and added 50 μg kanamycin per millilitre of medium. PET28a (+) has isolated recombinant plasmid from the colonies, restricted gene and cloned it. The LB agar plates containing 50 μg of kanamycin per millilitre medium were screened for successful transformation. The PCR colony and the restriction analysis confirmed the recombinant plasmid.

Based on the mutations suggested by the Structural Bioinformatics group at Fiocruz Ceará, the result of the work of Pacheco (2018), and following the methodology adapted from Edelheit, Hanukoglu & Hanukoglu (2009), mutagenic primers for insertion of mutations in the native ansB gene previously cloned into pET-28a expression vector were elaborated. The design of the mutagenic primers consisted of a region defined by

oligonucleotides that were complementary to each other, which contained the desired mutations, and another region of annealing to the vector used as a template, with the annealing nucleotide sequence being greater than the complementary one in order to make the annealing temperature of this region 5 to 10 °C higher (Liu; Naismith, 2008). This method produces longer primers than those commonly used in traditional gene amplifications. The mutations to be inserted are usually arranged in the complementary sequence of the mutagenic oligonucleotides, but it is also possible to arrange them in both regions, producing single, double, triple, quadruple or quintuple mutations.

The nucleotide sequences of the mutagenic primers designed for the development of this work will not be shown, as they are the intellectual property of Fiocruz groups and will soon be patented.

Polymerase Chain Reaction (PCR)

The commercial gene synthesized in pET-28a was amplified by PCR using 10 μM of pPET-28A Fw and Rv primers, 200 mM of dNTP, 1 U of GoTaq® DNA polymerase enzyme and its respective buffer (5x) and 10μL of genomic DNA (~150 ng) , for a final volume of 50 µL. The thermocycling parameters were set for 29 cycles following the scheme below for denaturation, DNA renaturation and primer annealing:

- 95˚C for 2 minutes.
- 95˚C for 1 minute.
- 52˚C for 1 minute.

Mutagenic PCR: For the production of the mutants, ansB-pET-28a template was used, added to the reaction 25 µL of HF buffer (5x), 2.5 µL of each Fw and Rv primer (10 µM), 4 µL of dNTPs Mix (200 mM final concentration), 1.5 µL dimethylsulfoxide (DMSO), 0.5 µL high fidelity Phusion enzyme (1 U), for a final reaction volume of 50 µL. The thermocycling parameters were set for 12 cycles following the scheme below for denaturation, DNA renaturation and primer annealing:

- 98˚C for 30 seconds.
- 60˚C for 30 seconds.

- 72˚C for 3 minutes and 30 seconds.

Plasmid digestion with restriction enzyme

Digestion with DpnI Enzyme: Digestion of approximately 12 µL of fined plasmid template (pET-28a-ansBm), previously subjected to mutagenic PCR, was carried out using 1 µL of the endonuclease enzyme DpnI (1 U), plus BSA (10x) and Multicore buffer (10x) for a final reaction of 20 µL. This reaction mixture was incubated for 2 hours at 37 °C, and the enzyme was inactivated at 70 °C for 15 minutes. Subsequently, all 5 µL of digested DNA plus 1 µL of sample buffer containing Gel-Red (diluted 5x) was subjected to 1% agarose gel electrophoresis (item 5.6) with 7 µL of 1 Kb molecular weight marker , and the sample of interest was purified from gel excised, as described in item 5.8.

Digestion with *Bam*HI and *Hind*III restriction enzymes: The expression vector pET-28a, which adds to the N-terminal portion of the protein expressing a PET-28A-Histag, was submitted to a digestion reaction with 1 µL of the endonucleases *Bam*HI and *Hind*III (10 U/each), adding the reaction (20 µL) of final volume) 2 µL of 10x Bovine Serum Albumin (BSA), 2 µL of Multicore buffer (10x) 1 µg of plasmid DNA, incubating the reaction for 3 hours at 37˚ C in a water bath. The restriction enzymes were inactivated by incubation for 15 minutes at 70˚C.

Then, the digested plasmid was subjected to enzymatic treatment with alkaline phosphatase (5U), where at 20µL of the digestion reaction 10x phosphatase buffer (10x) and 1µL of enzyme were added, for a final reaction volume of 25 µL. The reaction mixture was incubated at 37˚C for 1 hour, with enzyme inactivation at 65˚C for 15 minutes.

Subsequently, the entire content of digested DNA was added to sample buffer containing Gel-Red (diluted 5x) and subjected to a 1% agarose gel electrophoresis (item 5.6) with 7 µL of 1 Kb molecular weight marker. The sample of interest was purified from gel excised, as described in item 5.8, after quick visualization of the referred band in a transluminator.

Insert linking to plasmid vector

To calculate the amount of native ansB insert that should be used for a pET-28a vector binding reaction, the following equation was adopted (suggested by the DNA ligase A enzyme manufacturer).

From this calculation, 7 µL of pET-28a vector equivalent to approximately 100 ηg was added to 3 µL of ansB insert (80 ηg), 2 µL of ligase buffer (10x) and 1µL of ligase enzyme (1U), for a final volume 20 µl. The reaction was incubated at 4˚C overnight and the enzyme ligase was inactivated by heat treatment for 15 minutes at 65˚C.

Extraction of plasmid DNA (Miniprep)

The extraction of plasmid vectors used in this work was carried out using a commercial kit from Promega® Wizard Plus SV Minipreps DNA Purification Systems, following instructions contained in the manufacturer's manual. After performing this experimental stage, the plasmids were quantified in a NanoDrop device (ThermoScientific®).

Bacterial competence by chemical method

The bacterial strains of *E. coli* JM103 and Rosetta were subjected to chemical competence by stressing with saline solutions of $MgCl_2$ (0.1 M) and $CaCl_2$ (0.1 M). Pre-inoculums of each strain, from isolated colonies, were prepared in Luria Bertani Broth Miller (LB) medium without antibiotics, in volumes of 5 mL and incubated under agitation (200 rpm) at 37 °C, overnight. In 300 mL of antibiotic-free LB, 5 mL of each pre-inoculum were added, which were incubated at 37 °C and 200 rpm until they reached optical density (OD) at 600 µm of 0.5 (approximately 3 hours) .

Once the O.D. was reached, the bacterial culture volume was centrifuged at 4 °C for 10 minutes at 5000 x g, and, reserving only the cell pellet (pellet), for cell resuspension with 40 mL of ice-cold $MgCl_2$. This was followed by a new centrifugation at 4°C, 3000 x g for 10 minutes and, subsequently, the supernatant was discarded. The pellet was resuspended again, this time with 2 mL of cold $CaCl_2$, leaving the bacteria to rest for 20 minutes on

ice, followed by the addition of 1 mL of 25% glycerol. 100 μL aliquots were placed in previously chilled 1.5 mL tubes and stored at -80 °C.

Results and Discussion

The positioning of the four mutations carried out in the monomeric structure of the protein is shown in Figure 1. It is observed that mutations 1 and 2 that make up the double-mutant produced are closer to the catalytic site than the others. Therefore, its interatomic interaction potential (PII) between the amino acids of the catalytic site, the residues of two mutations 1 and 2 and the substrate was calculated.
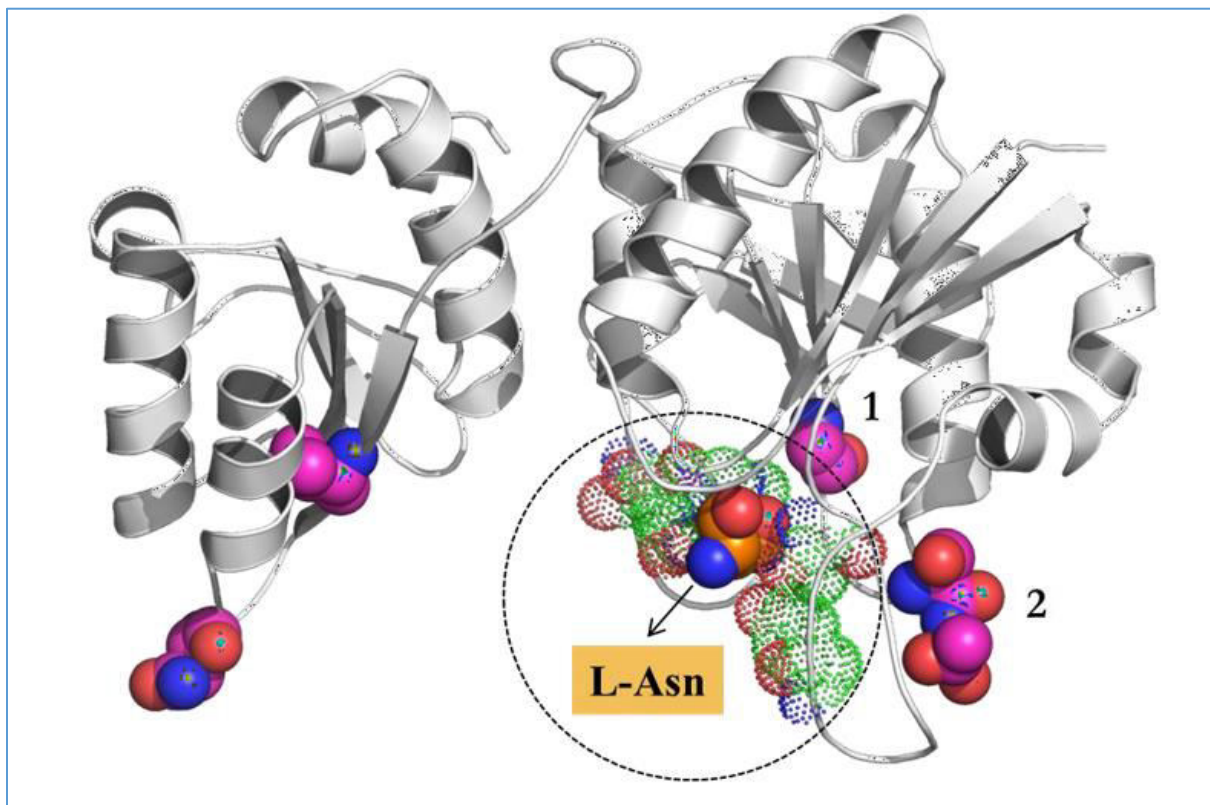
Figure 1. Representation of JM103 L-ASP monomer with spatial locations of mutations [Prepared by the author. JM103 L-ASP monomer with emphasis on residues in spheres with carbon colored in pink and the region of the catalytic site circled in red dots, in addition to residues from the site represented in dots with carbon colored in green. L-Asn substrate at the center of the catalytic site represented in a sphere with orange colored carbon]

The PII profile between the l-Asn substrate and mutation I (G113D) in the double-mutant system, in each monomer (A, B, C and D), is shown in Graph 2. In the native system, it is possible to infer that glycine (G113) did not interact with the l-Asn substrate at the site, since the energy is at the imminence of zero during the entire simulation time. In the double-mutant system, it can be seen that the exchange for an aspartic acid (D113) in the same position started to interact considerably with the substrate of the site, as shown in graph 2II, evidenced by the black curves (monomer A) and pink (monomer D). The apparently opposing profile of the black and pink curves indicates the alternating character of the interaction, sometimes attractive and sometimes repulsive with l-Asn, which disturbs the correct orientation of the substrate in the active site and causes damage to the catalytic activity of the enzyme.
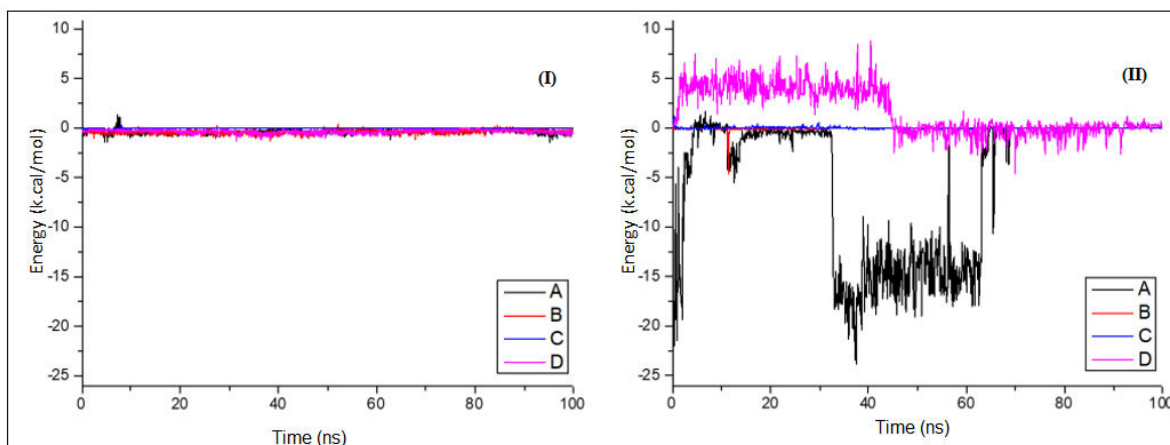
Graph 2. Interatomic interaction potential curve between l-Asn substrate and mutation 1 residue in each JM103 L-ASP monomer [Prepared by the author. Cure of PII showing the interaction behavior between the substrate l-Asn and the residues of mutation 1 (G113D). (I) Native system, where residue is a Glycine. (II) Double-mutant system, where the residue is an Aspartic Acid]

This disturbance becomes even clearer when looking at Graph 3, where it is possible to observe the PII profile between the residues of the catalytic site, in the native system (Graph 3I) and in the double-mutant (Graph 3II), respectively. In the double-mutant

system, the replacement of glycine by aspartic acid allowed an attractive interaction between it and the residues of the site, corresponding to an energy of approximately -36 kcal.mol-1 in monomer A. This attraction behavior resulting from the mutation could explain the low catalytic activity of the mutant, since
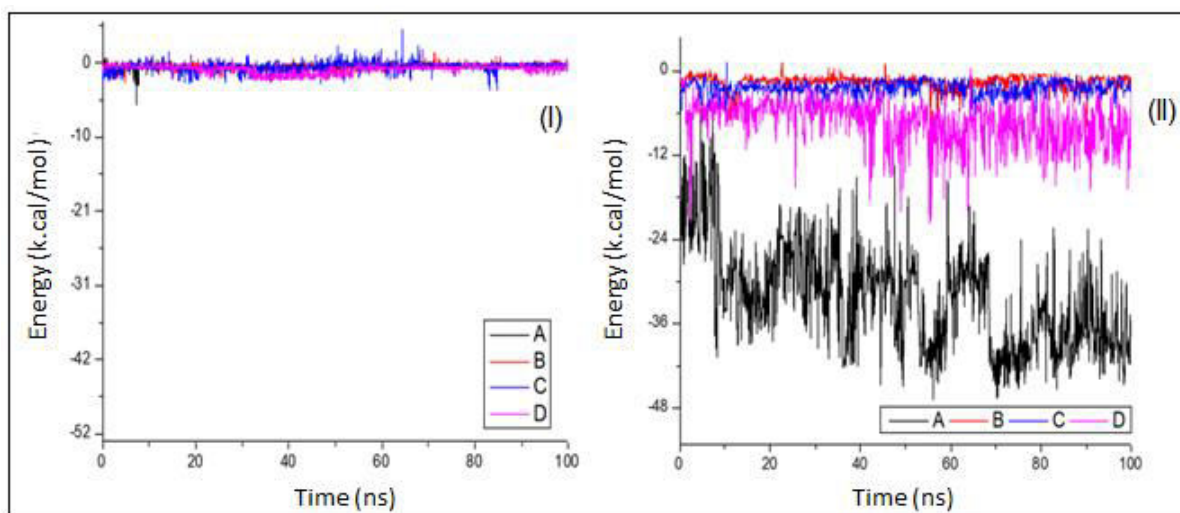
Graph 3. Interatomic interaction potential curve between residues from the catalytic site of JM103 L-ASP and mutation 1 that would impact the interaction of the substrate with the residues of the catalytic site.

Figure 2 shows the region of the active site of JM103 L-ASP, both in the native system and in the double-mutant, in the initial configurations and at 50 ns, which is the time in which an attractive interaction is observed between the residue Aspartic acid and l-Asn in monomer A (black curve in graph 2 II), of approximately -15 kcal/mol.
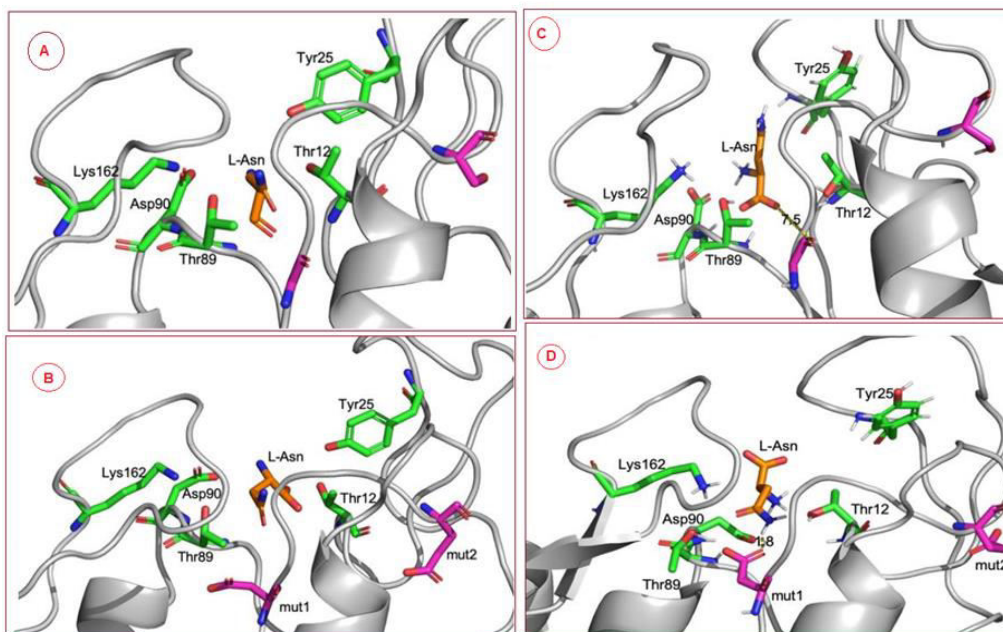
Figure 2: Spatial representation of catalytic residues in one of the JM103 L-ASP monomers in the presence of l-Asn substrate [Source: Prepared by the author. Spatial representation of the component residues of the JM103 L-ASP active site (represented in stick and colored carbons in green) in the presence of the substrate l-Asn at the center of the site (carbon in orange). The native and double-mutant protein residues, containing mut1 and mut2, are colored pink. (A) Initial setup on native system. (B) Initial setup in double-mutant system. (C) Configuration after 50 ns simulation in the native system, highlighting the distance between the G113 residue and the l-Asn substrate (7.5 Å). (D) Configuration after 50 ns simulation in the double-mutant system, highlighting the distance between the D113 residue and the l-Asn substrate (1.8 Å)]

In order to assess whether the S118E mutation (mutation 2) would also cause perturbation in the catalytic site region, the PII between the L-Asn substrate and the substitute amino acid was calculated, both in the native and in the double-mutant system, as it is possible to observe in graph 4. Comparing the interaction profile between the amino acid Serine present in the native configuration of JM103 L-ASP to that evidenced by the substituted Glutamic Acid, notably, mutation 2 alone was not able to vary the potential of interaction with the substrate to the point of impacting on the activity enzyme

catalytic effect, since in both graphs the potential remains close to zero throughout the simulation. Therefore, there is no interference in the orientation of l-Asn at the site or in catalysis with the presence of mutation 2.
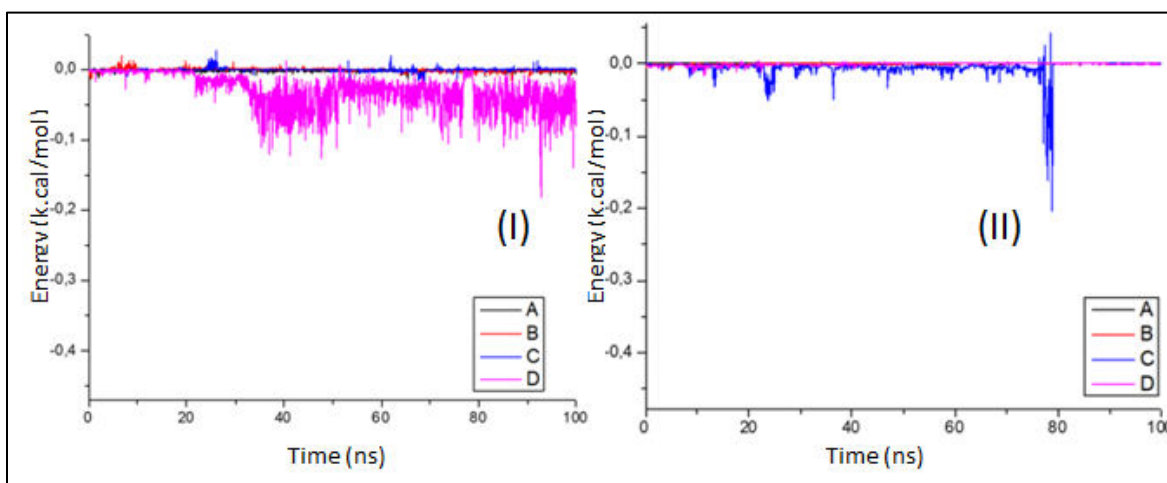
Graph 4. Interatomic interaction potential curve between l-Asn and mutation 2 in each JM103 L-ASP monomer [Prepared by the author. PII curve between the substrate l-Asn and S118 in each monomer (A, B, C and D) of JM103 L-ASP, where (I) represents the interactive potential profile of the native system, with amino acid Serine at position 118, and (II) the double-mutant system, where the substitute residue at position 118 is a Glutamic Acid]

Graph 5 shows the potential between the atoms that constitute the catalytic site residues and those of the substitute E118 residue, both in the native and double mutant systems. It is noticed that glutamic acid shows attractive power with amino acids from the site, reaching -8 kcal.mol-1 in some monomers. The wild residue (serine) also has attractive potential, however at a lower value: around -5 kcal/mol. Therefore, the inserted mutation 2 would not justify the loss of activity, since the interaction pattern was maintained and there are no abrupt changes in the potential.

Furthermore, it can be seen in Figure 3 D that the substitute residue (glutamic acid) has its side chain facing the solvent, which makes this residue possibly not disturb the catalytic site interactions necessary for catalysis.
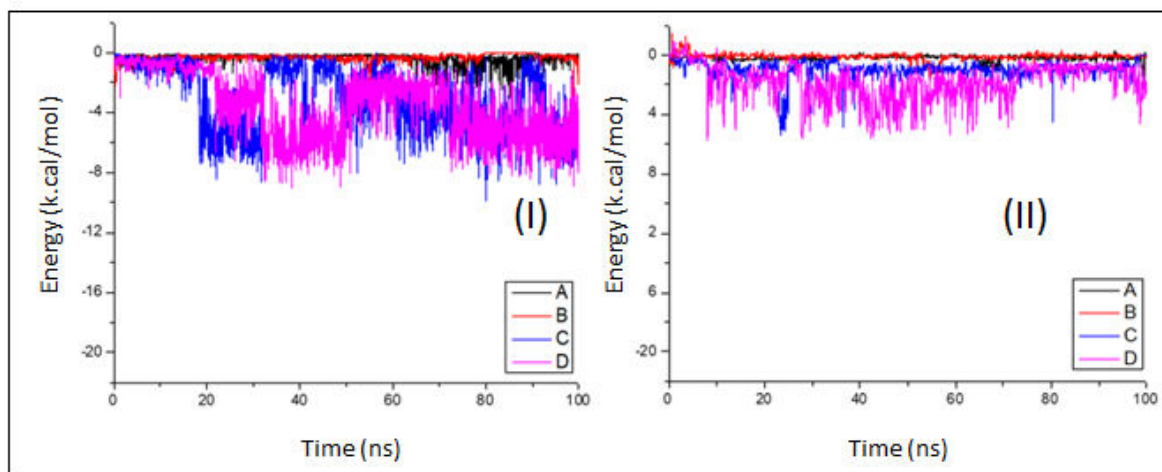
Graph 5. Interatomic interaction potential curve between residues from the catalytic site of JM103 L-ASP and mutation 2. [Prepared by the author. PII curve between the group of atoms that constitute the residues of the catalytic site of JM103 L-ASP and the residue E118 of mutation 2 over the simulation time in each monomer (A, B, C and D). Where (I) corresponds to the native system and (II), double-mutant system]

Based on these data, we started to verify the impact of mutation 1 (G113D) reversal as a sufficient alternative for the modified protein to return to present catalytic activity corresponding to the native one. For this, the other mutations present in the quadruple-mutant system were evaluated. Graph 6 shows the PII between the l-Asn and the group of atoms that constitute the mutated residues in both the native and the quadruple-mutant systems. Through the analysis of the mutant in question, we can infer that there is no considerable variation in the interaction of these residues since, in both systems, the interaction potential is very close to zero during the entire simulation time, with the lowest energy observed in the quadruple-system. mutant (kcal/mol), approximately.
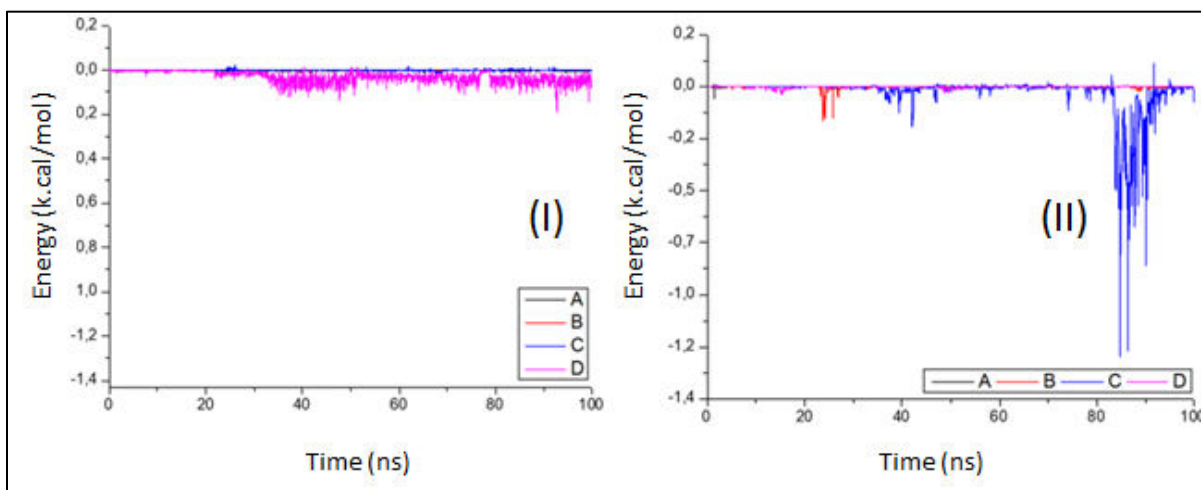
Graph 6. Interatomic interaction potential curve between the l-Asn substrate and each surrogate residue in the quadruple-mutant system of JM103 L-ASP, except for mutation 1. [Prepared by the author. PII curve between the l-Asn and the component residues of each mutation of the quadruple-mutant, except for mutation 1, where (I) corresponds to the interaction profile in the native system and (II) the interaction profile in the quadruple-mutant system containing mutation 2 and three other mutations produced *in vitro* in this work]

Graph 7 shows the PII between the group of atoms that form the catalytic site residues and those that constitute the exchanged residues in both the native and the quadruple-mutant systems. Note that for both systems, the energy remains negative throughout the simulation, so the attractive potential between these groups
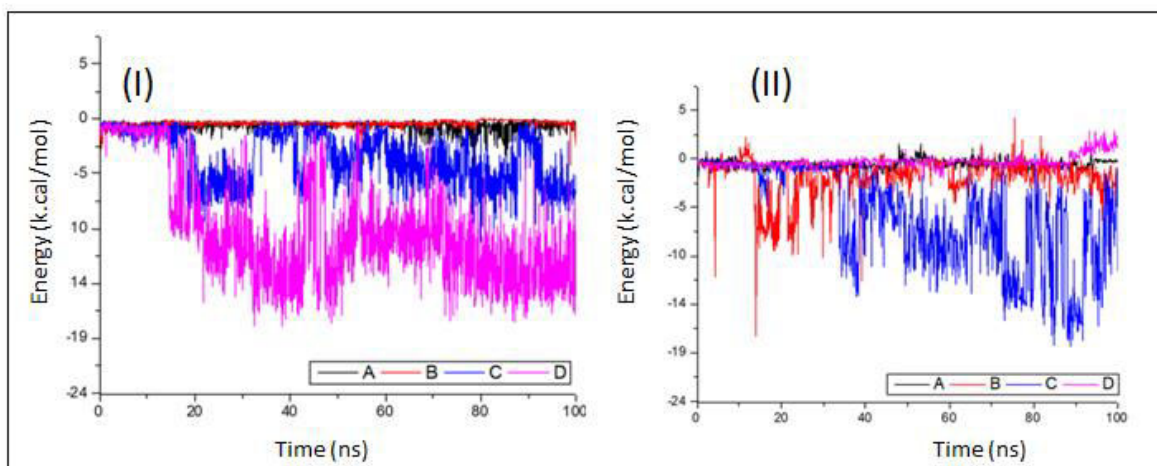
Graph 7. Interatomic interaction potential curve between catalytic site residues and substitute residues in the quadruple-mutant of JM103 L-ASP, except for mutation 1 [Prepared by the author. PII curve between the group of atoms that form the residues of the catalytic site of JM103 L-ASP and the group of atoms that constitute the mutated residues over the simulation time in each monomer (A, B, C and D) of the tetramer structure. (I) Native system. (II) Quadruple-mutant system, with four mutations, except mutation 1 of atoms is kept]

In both systems there is a monomer that differs from the others: monomer D, pink curve in the native system, and monomer C, blue curve in the quadruple-mutant system. However, energy is maintained at an average of approximately -12 kcal/mol in both monomers. Such variation would not justify the loss of activity in these mutants, therefore, the loss of enzymatic activity was probably caused only by mutation 1 (G113D).

Since the mutated residues, except mutation 1 (G113D), are not located in regions close to the site (figure 3) or are not influencing the interactions necessary for catalysis (graphs 4, 5, 6 and 7), a future perspective it would be the reversal of mutation 1 and the performance of new activity tests.

Conclusion

In this study, the regulation of enzyme production was studied by culturing bacteria in poor and rich nutrient media containing various carbon and nitrogen sources, under different pH and temperature conditions. In addition, how this regulation occurs in recombinant bacteria was also investigated comparatively.

References

Gomes, D. C. Biochemical and kinetic characterization of bacterial L-asparaginases and evaluation of their cytotoxic potential, Course Conclusion Paper, Federal University of Ceará, Fortaleza, 31 f. 2019.

Jawa, V.; Cousens, L. P.; Awwad, M.; Wakshull, E.; Kropshofer, H.;Groot, A. S. D. T-cell dependent immunogenicity of protein therapeutics: Preclinical assessment and mitigation. Clinical Immunology, Elsevier, v. 149, p. 534–555, 2013.

Kumar, K., Verma, N., The various sources and application of L-asparaginase. Asian Journal of Biochemical and Pharmaceutical Research, v. 2, n. 3, p. 197–205, 2012.

Lopes A. M., Oliveira-Nascimento L., De Ribeiro A., et al. Therapeutic l-asparaginase: upstream, downstream and beyond. Crit Rev Biotechnol, v. 8551, p. 1- 18, dec. 2015.

Nelson, D.L.; COX, M.M. Lehninger's Principles of Biochemistry. 5. ed. Porto Alegre: Artmed, 2011.

Pacheco, D.L.A. Deimmunization of L-asparaginase from Escherichia coli by Genetic Algorithm. Course Completion Paper, Federal University of Ceará, Fortaleza, 86 f. 2019.

Salzer, W. L., Asselin, B. L., Plourde, P. V., Corn, T., Hunger SP. Development of asparaginase Erwinia chrysanthemifor the treatmentof acute lymphoblastic leukemia. Annals of the New York Academy of Sciences, v. 1329, p. 81–92, 2014.

Shen, Y.; Maupetit, J.; Derreumaux, P.; Tuffery, P. Improved PEP-FOLD Approach for Peptide and Miniprotein Structure Prediction. Journal of Chemical Theory and Computation, [S.l.], v. 10, p. 4745–4758, 2014.

Verma N., Kumar K., Kaur G., Anand S. L-asparaginase: a promising chemotherapeutic agent. Crit Rev Biotechnol, v. 27, n. 1, p. 45-62, out. 2007. Disponível em: http://dx.doi.org/10.1080/07388550601173926.

Yao, H., Wynendaele, E., De Spiegeleer, B. Thermal sensitivity as a quality control attribute for biotherapeutics: The L-asparaginase case. Drug Test Anal; 1–11. 2019.

Yazdi, Mehdi & Kolahi, Maryam & Foroghmand, A. & Tabandeh, Mohammad reza. (2020). In silico assessment of plant L-asparaginase and estimating its allergenicity in comparison to bacteria asparaginase. Pediatric Hematology/Oncology and Immunopathology. 19. 35-46. 10.24287/1726-1708-2020-19-1-35-46.

Zhao, H.; Verma, D.; Li,W.; Choi, Y.; Ndong, C.; Fiering, S. N.; Bailey-Kellogg, C.; Griswold, K. E. Depletion of T cell epitopes in lysostaphin mitigates anti-drug antibody response and enhances antibacterial efficacy *in vivo*. Chemistry and Biology, Elsevier, v. 22, p. 629–639, 2015.